Observation of Bifurcations and Hysteresis in Nonlinear NbN Superconducting Microwave Resonators

Baleegh Abdo, *Student Member, IEEE*, Eran Arbel-Segev, Oleg Shtempluck, and Eyal Buks

***Abstract*—In this paper, we report some extraordinary nonlinear dynamics measured in the resonance curve of NbN superconducting stripline microwave resonators. Among the nonlinearities observed: aburpt bifurcations in the resonance response at relatively low input powers, asymmetric resonances, multiple jumps within the resonance band, resonance frequency drift, frequency hysteresis, hysteresis loops changing direction and critical coupling phenomenon. Weak links in the NbN grain structure are hypothesized as the source of the nonlinearities.**

***Index Terms*—Bifurcations, hysteresis, jumps, microwave resonators, nonlinear effects, NbN.**

I. Introduction

NONLINEAR effects in superconductors in the microwave regime have been the subject of a large number of intensive studies in recent years. Most of the attention is focused on studying one or more of the following issues: investigating the origins of nonlinear effects in superconductors [1], [2], introducing theoretical models that explain nonlinear behavior [3], [4], identifying the dominant factors that manifest these effects [5], [6], find ways to control and minimize nonlinear effects [7], [8] such as, harmonic generation and intermodulation distortions, which degrade the performance of promising superconducting microwave applications mainly in the telecommunication area [9].

Among the nonlinear effects reported in the literature associated with resonance curves, one can find the commonly known Duffing oscillator nonlinearity which is characterized by skewed resonance curves above certain power level, appearance of infinite slope in the resonance lineshape, pronounced shift of the resonance frequency and hysteretic behavior [10]–[12]. To account for this effect, associated with the rise of kinetic inductance of superconductors, both thermal [13], and weak link [10] explanations have been successfully applied. Other nonlinear effects were reported by Portis *et al.* [14], where they observed notches that develop on both sides of the frequency response of their high-temperature superconducting (HTS) microstrip patch antenna, accompanied with hysteresis and frequency shift, in the nonlinear regime. Similar results were reported also by Hedges *et al.* [15], in their YBCO stripline resonator, and in [16] in YBCO thin film dielectric cavity. All three studies [14]–[16] attributed the observed nonlinear behavior to abrupt changes in the resistive loss of weak links, thermal quenching, and weak link switching to normal state.

In this study, being interested in the behavior of nonlinear resonances, we have fabricated different NbN superconducting microwave resonators exhibiting some unusual nonlinear effects, which to the best of our knowledge, have not been reported before in the literature. We study the dependence of these resonators on input power, and examine the resonance curve behavior under different scan directions. To account for our results, we consider some possible physical mechanisms which may be responsible for the observed effects.

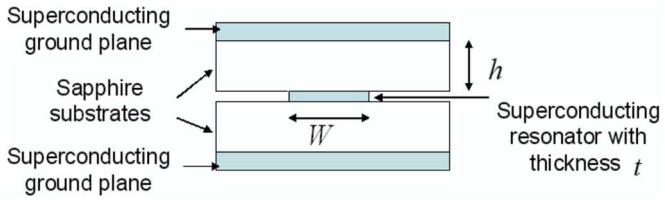

Fig. 1. Stripline geometry.

II. Resonators Design

The resonators were designed in the standard stripline geometry, which consists of five layers, as shown in the cross-section illustration, depicted in Fig. 1.

The superconducting resonator was dc-magnetron sputtered on one of the sapphire substrates, whereas the superconducting ground planes were sputtered on the inner covers of a gold plated Faraday package made of oxygen free high conductivity (OFHC) copper employed to house the resonators. The dimensions of the sapphire substrates were $34 \times 30 \times 1$ mm. The resonator geometries implemented, which we will refer to them, for simplicity, by the names B1, B2, and B3, are presented in the insets of Figs. 3–5 respectively. The width of the feedlines and the thin part of the resonators was set to 0.4 mm to obtain characteristic impedance of 50 Ω. The gap between the feedline and the resonators was set to 0.4 mm in B1, B3 cases, and to 0.5 mm in B2 case. The frequency modes of B1, B2, B3 resonators were theoretically calculated using a simple transmission line model, presented in Appendix A, and were also experimentally

Manuscript received January 9, 2005; revised June 28, 2005. This paper was recommended by Associate Editor J. Mazierska. This work was supported by the German Israel Foundation under Grant 1-2038.1114.07, by the Israel Science Foundation under Grant 1380021, and by the Deborah Foundation and Poznanski Foundation.

The authors are with the Department of Electrical Engineering and Microelectronics Research Center, Technion, Haifa 32000, Israel (e-mail: baleegh@tx.technion.ac.il).

Color versions of Figs. 1–5, Figs. 7–10 and Figs. 13–15 are available online at http://ieeexplore.ieee.org.

Digital Object Identifier 10.1109/TASC.2006.881823

TABLE I
SPUTTERING PARAMETERS

Process parameter	B1	B2	B3
Partial flow ratios (Ar,N2)	(87.5%,12.5%)	(75%,25%)	(70%,30%)
Base temperature	11 °C	11 °C	13 °C
Total pressure	$6.9 \cdot 10^{-3}$ torr	$8.1 \cdot 10^{-3}$ torr	$5.7 \cdot 10^{-3}$ torr
Discharge current	0.36A	0.55A	0.36A
Discharge voltage	351V	348V	348V
Discharge power	121W	185W	133W
Deposition rate	$6\frac{\text{Å}}{sec}$	$7.8\frac{\text{Å}}{sec}$	$3.8\frac{\text{Å}}{sec}$
Thickness (t)	2200 Å	3000 Å	2000 Å
Base pressure	$3.1 \cdot 10^{-8}$ torr	$7.3 \cdot 10^{-8}$ torr	$8 \cdot 10^{-8}$ torr
Target-substrate distance	80mm	90mm	90mm

measured using vector network analyzer (NA). The theoretical calculation was found generally to be in good agreement with the measurement results, as discussed in Appendix A.

III. FABRICATION PROCESS

The sputtering of the NbN films was done using a dc-magnetron sputtering system. All of the resonators reported here were deposited near room temperature [17]–[19], where no external heating was applied.

The system was usually pumped down prior to sputtering to $3\text{–}8 \cdot 10^{-8}$ torr base pressure (achieved overnight). The sputtering was done in Ar/N_2 atmosphere under current stabilization condition [20]. The relative flow ratio of the two gases into the chamber and the total pressure of the mixture were controlled by mass flow meters. The sputtering usually started with a -min presputtering in the selected ambient before removal of the shutter and deposition on the substrate. The sputtering parameters of the three resonators are summarized in Table I. Following the NbN deposition, the resonator features were patterned using standard photolithography process, whereas the NbN etching was done using Ar ion-milling.

To obtain resonators with reproducible physical properties we have used the sputtering method discussed in [20] and [21], where it was claimed that reproducible parameters of films are assured, by keeping the difference between the discharge voltage in a gas mixture and in pure argon, constant, for the same discharge current. In Fig. 2, we show one of the characterization measurements applied to our dc-magnetron sputtering system, exhibiting a knee-shape graph of discharge current as a function of discharge voltage. The knee-shape graph was obtained for different Ar/N_2 mixtures at room temperature. The discharge voltage difference measured in the presence of N_2 gas relative to the value measured in pure argon at the same discharge current, is also pointed out in the figure, corresponding to different currents and N_2 percentages.

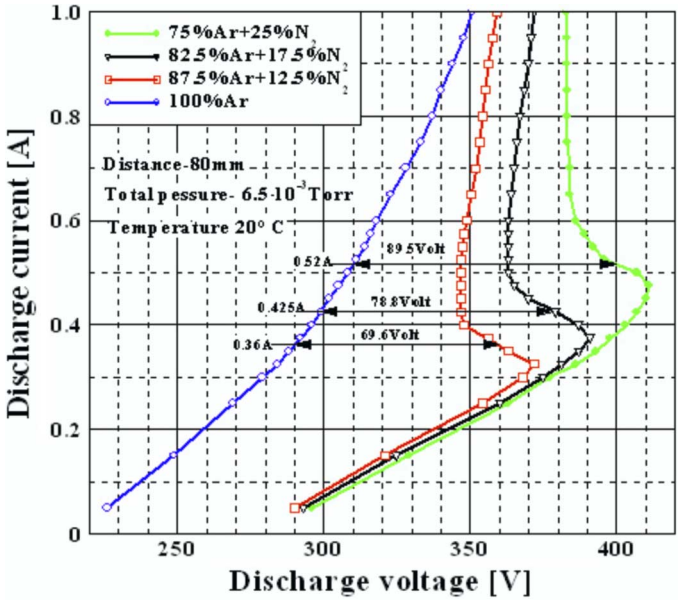

Fig. 2. Discharge current versus discharge voltage of the sputtering system displaying current-voltage knee for different percentages of Argon and Nitrogen, at ambient temperature of 20°C.

IV. PHYSICAL PROPERTIES

The fabricated resonators were characterized by relatively low T_c for NbN and relatively intermediate resistivity ρ. Resistance measurements were performed using standard four probe technique. T_c measured for B1, B2 and B3 was 10.7, 6.8, 8.9 [K] respectively, whereas ρ measured was 348 and 500 $[\mu\Omega]$ cm for B2 and B3, respectively. Critical temperature width ΔT_c measured for B3 resonator yielded 0.5 K (where ΔT_c is defined by the 5% and 95% points of the resistive transition), which may indicate that the intergrain Josephson coupling in this film is still dominant compared to granular behavior [22]. Residual resistance ratio (RRR) defined as $\rho(300)/\rho(15)$, where $\rho(300)$ refers to resistance value at room temperature and $\rho(15)$ refers to resistance before superconducting transition, was also measured for B3 resonator and yielded RRR of 0.5. This less than unity low RRR ratio, indicating a granular or columnar (island) structure [17] and nonmetallic conduction [18], [23], is in good correlation with the relatively low T_c (8.9 K) and high resistivity ρ (500 $\mu\Omega$ cm), measured for this film [18]. In addition, RRR ratios less than unity, implying a negative temperature coefficient of resistivity (TCR) [24] (the resistance increases with decreasing temperature), generally characterizes NbN films having a columnar (island) structure [24]. Moreover, these measured parameters $T_c, \Delta T_c, \rho$ and RRR ratio are in good agreement with the results of [22] and [18], where it was shown that increasing the partial pressure of N_2 in Ar/N_2 mixture at a given total pressure tends to decrease RRR ratio and T_c, and increase ρ and ΔT_c. The relatively low T_c measured, can be attributed also to bulk degradation and vacancies [22], or more likely to columnar grain boundaries [25]. Furthermore, from scanning electron microscopy micrographs taken to a NbN film sample sputtered with similar sputtering conditions as B2 resonator, and showing a clear columnar structure of the kind discussed in [24]–[26],

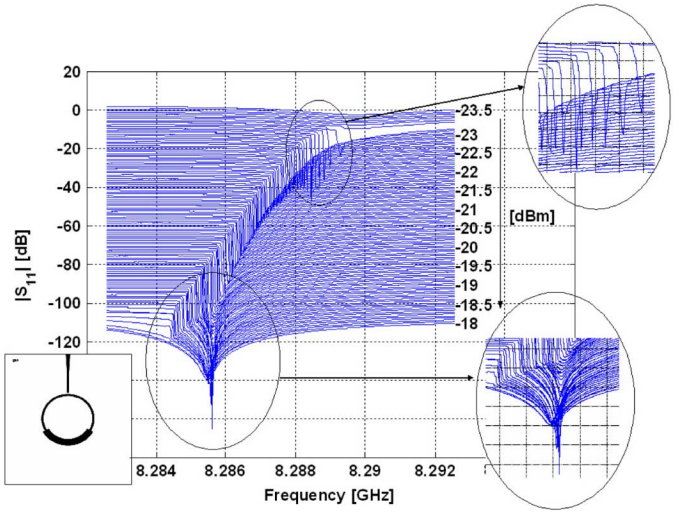

Fig. 3. S_{11} measurement of B1 resonance at ~ 8.288 GHz with 10-MHz span, exhibiting extraordinary nonlinear effects at low input powers. Resonance curves corresponding to different input powers were shifted by a constant offset for clarity.

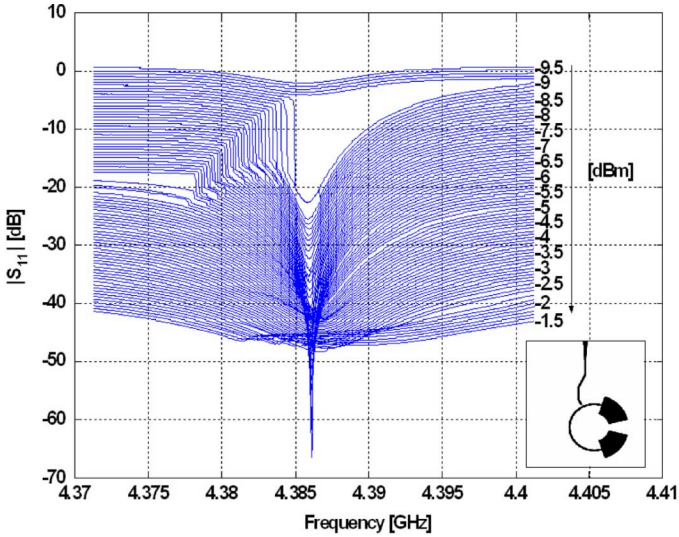

Fig. 4. S_{11} measurement of B2 resonance at ~ 4.385 GHz with 30-MHz span, exhibiting strong nonlinear effects at low input powers. Resonance curves corresponding to different input powers were shifted by a constant offset for clarity.

one can estimate the diameter of the columnar structure to be of the order of 20 nm.

V. Measurement Results

All measurements presented in this paper have been conducted at liquid helium temperature 4.2 K, and were verified using two cryogenic configurations. One was by immersing the resonator package in liquid helium, two by housing the resonator package in vacuum inside a temperature controlled cryostat. No significant differences were detected in the experimental data measured using these two cryogenic techniques.

A. S_{11} Measurements

The resonance response of the resonators was measured using the reflection parameter S_{11} of a NA. The resonance response obtained for the third mode of B1 resonator ~ 8.288 GHz at low input powers, between -23 dBm and -18 dBm in steps of 0.05 dBm, is shown in Fig. 3. A small vertical offset was applied for clarity between the sequential graphs corresponding to different input powers and to show the nonlinear evolution of the resonance response as the input power is increased. The interesting characteristics of this nonlinear evolution can be summarized as follows.

1) In the power range between -23.5 dBm and -23.25 dBm, the resonance is symmetrical and broad.
2) At input power level of -23.25 dBm, a sudden jump of about -15 dB occurs in the resonance curve at the minima where the slope of the resonance response is small.
3) As the input power is increased in steps of 0.05 dBm the resonance becomes asymmetrical, and the left jump shifts towards lower frequencies gradually.
4) As we continue to increase the input power, the jumps decrease their height but the resonance curve following the jumps becomes more symmetrical and deeper, and at a certain input power level we even witness a critical coupling phenomenon where $S_{11}(\omega)$ at resonance is almost zero, that is no power reflection is present.
5) The resonance becomes symmetrical again and broader and the jumps disappear.
6) All previously listed effects occur within a frequency span of 10 MHz, power range of about 5 dBm, and power step of 0.05 dBm.

Similar behavior to that exhibited by the nonlinear third mode of resonator B1 can be clearly seen in Figs. 4 and 5, which show the nonlinear dynamic evolution of the second mode of resonator B2 and the first mode of B3 respectively. The main differences between the figures are:

1) The power levels at which these nonlinear effects appear. Whereas in B1 case they happen between -23 dBm and -18 dBm, in B2 case they happen between -9.5 dBm and -1.5 dBm and in B3 case they happen around 1 dBm.
2) In Fig. 5 corresponding to B3 resonator we witness three apparent jumps within the resonance band as indicated by circles shown on the figure, a feature that we did not encounter in Figs. 3 and 4.

In order to evaluate approximately the peak RF magnetic field H_{RF} at the surface of the stripline, associated with the onset of nonlinearity of the resonances shown in Figs. 3 and 4, we apply the calculation method described in [27], [28] for a uniform resonator, with the necessary changes to account for the one port configuration and the nonuniform current density at the edges. The maximum RF current of the standing waves at resonance in a uniform resonator is given by $I_{\max} = \sqrt{(1-r_v^2)8QP_W/n\pi Z_0}$, where r_v is related to the return loss R measured in [dB] given by $R = -20\log_{10} r_v$, where Q is the unloaded quality factor of the stripline (to obtain an order of magnitude of H_{RF} we assume $Q_L \sim Q$), P_W is the incident power, n is the mode number of the resonance measured, and Z_0 is the characteristic impedance of the transmission line $\sim 50\ \Omega$. Thus, the peak of the RF magnetic field H_{RF} at the edges of the strip associated with $I_{\max}$, can be evaluated by accounting for the nonuniform current density along the cross section of the strip and by applying Ampere's

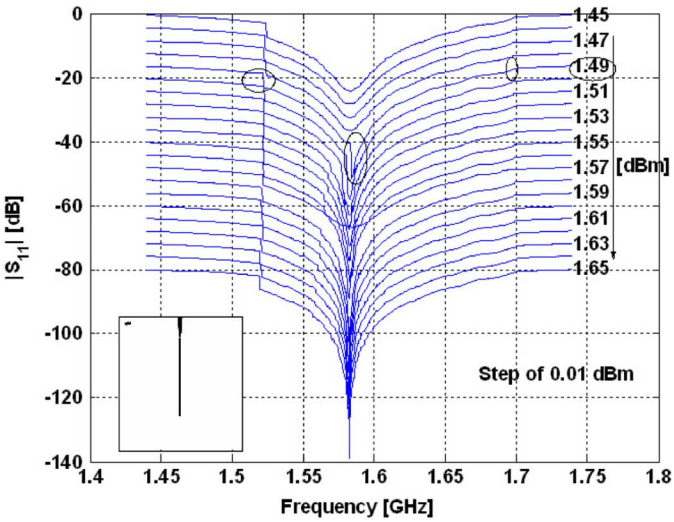

Fig. 5. Nonlinear response of B3 resonance at ~ 1.6 GHz, corresponding to input power levels increasing by a 0.01 dBm step. At input power of 1.49 dBm, we observe two obvious jumps in the resonance band, and another small one at the right side, marked with circles. The different resonance curves were shifted by a constant offset for clarity.

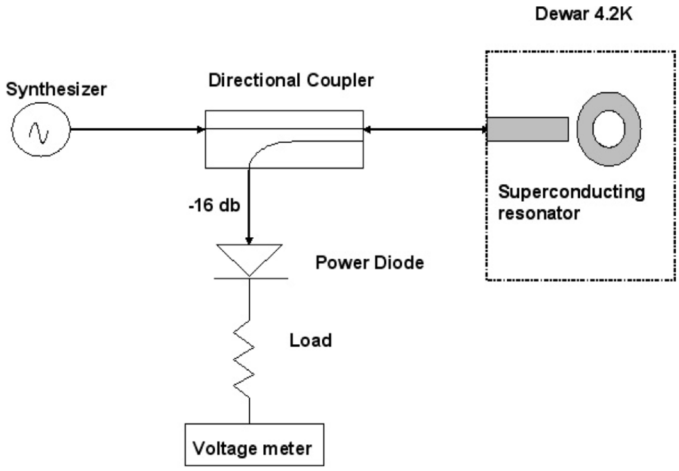

Fig. 6. Setup used to verify the occurrence of the bifuractions at the nonlinear resonance (B1 third mode) previously measured by NA.

law at the edges. A relatively good approximation for the nonuniform current density of a thin isolated strip of width W and thickness t is given by [29]

$$J(x) = \begin{cases} \frac{J(0)}{\sqrt{1-\left(\frac{2x}{W}\right)^2}}, & |x| \le \frac{W}{2} - \frac{\lambda^2}{2t} \\ J\left(\frac{W}{2}\right)\exp\left\{-\frac{t}{\lambda^2}\left(\frac{W}{2}-x\right)\right\}, & \frac{W}{2} - \frac{\lambda^2}{2t} < |x| \le \frac{W}{2} \end{cases} \quad (1)$$

where $J(W/2) = \exp(1/2)\sqrt{Wt}J(0)/\sqrt{2}\lambda$, λ is the London penetration depth, $J(0)$ is the current density at the middle of the strip.

In the following calculations, λ is assumed to be comparable to the thickness of the strip $t(t \simeq \lambda)$ (since λ of NbN is typically in the range of 2000–4000 unit Å [30]), whereas W the width of the strip is assumed to be the width of the narrowest part of the film 0.4 mm. Substituting the following values for B1 resonator at the onset of nonlinearity shown in Fig. 3, $P_{\rm dBm} = -23$ dBm, $R = 30$ dB, $Q \sim 7000, n = 3$, yields the following approximate peak RF magnetic field at the narrowest part $H_{\rm RF}\sim 6$ Oe. Whereas for B2 second resonance shown in Fig. 4, one gets $H_{\rm RF}\sim 9$ Oe, which corresponds to the following parameters, $P_{\rm dBm} = -9$ dBm, $R = 20$ dB, $Q\sim 462, n = 2$.

Moreover, by comparing the onsets of nonlinearity corresponding to the different resonance frequencies one finds different values even for the same resonator. Whereas, in B1 resonator, the onset of nonlinearity for the third resonance (~ 8.288 GHz) is about $I_{\rm max}\sim 24$ mA (~ 6 Oe), the onset of nonlinearity for the first resonance (~ 2.59 GHz) is much lower, $I_{\rm max}\sim 9$ mA (~ 2 Oe). In B2 resonator, whereas the second resonance frequency (~ 4.385 GHz) exhibited strong nonlinear behavior at about $I_{\rm max}\sim 40$ mA (~ 9 Oe) of the kind shown in Fig. 4, the first resonance frequency (~ 2.52 GHz) exhibited similar but smaller jumps at about $I_{\rm max}\sim 104$ mA (~ 23 Oe). In B3 resonator, the onset of nonlinearity for the first resonance is about $I_{\rm max}\sim 61$ mA (~ 17 Oe) (not shown in Fig. 5), whereas other resonances of this resonator exhibited nonlinearities at much lower currents about $I_{\rm max}\sim 4$ mA (~ 1 Oe).

These relatively low RF currents and magnetic fields, at which the nonlinear effects appear in the NbN films, are orders of magnitude lower than the magnetic fields generally reported in the literature, see for example [28], [31]–[33] , but they are, on the other hand, on the order of RF magnetic fields associated with Josephson vortices in YBCO grain boundaries reported for example in [34] and [35].

B. Verifications

In order to verify that the jump feature, previously measured using NA S_{11} parameter, is not a measurement artifact, we have applied a different measurement configuration, shown in Fig. 6, where we swept the frequency of a synthesizer and measured the reflected power from the resonator using a power diode and a voltage meter. The load that appears in Fig. 6 following the diode is used in order to extend the linear regime of the power diode. The results of this measurement configuration are shown in Fig. 7. The frequency scan around the resonance was done using 201 points in each direction (forward and backward). A small hysteresis loop is visible in the vicinity of the two jumps.

C. Abrupt Jumps

In attempt to find out whether the resonance curve of these nonlinear resonances changes its lineshape along two or more frequency points, further measurements where carried out using NA, where we scanned the frequency axis in the vicinity of the jump with high frequency resolution. The measurement results corresponding to frequency step of ~ 600 Hz and ~ 2.5 kHz are presented in Fig. 8(a) and (b), respectively, indicating abrupt transition between two bistable states.

D. Frequency Hysteresis

Bifurcations in the resonance response of the device usually occur when the resonance curve becomes multiple valued as a function of the drive frequency. Such multiple valued resonance

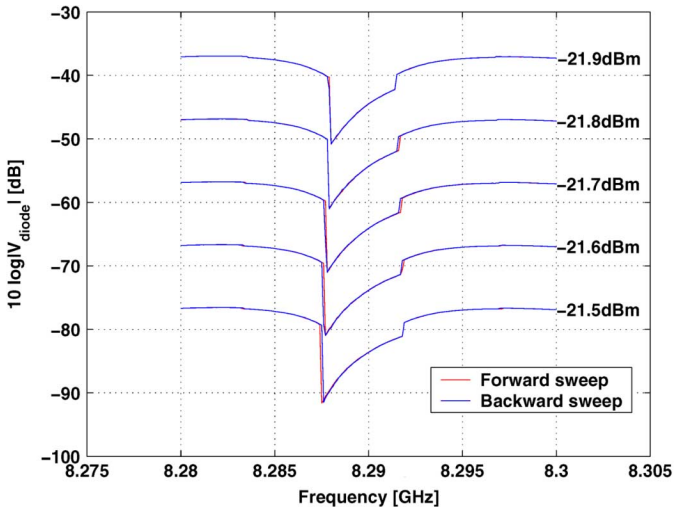

Fig. 7. Nonlinear response of B1 third mode measured using the configuration shown in Fig. 6. Red line represents a forward scan whereas the blue line represents a backward scan. Two abrupt jumps appear at both sides of the resonance curve and small hysteresis loops are present at the vicinity of the jumps. Resonance curves corresponding to different input powers were shifted by a constant offset for clarity.

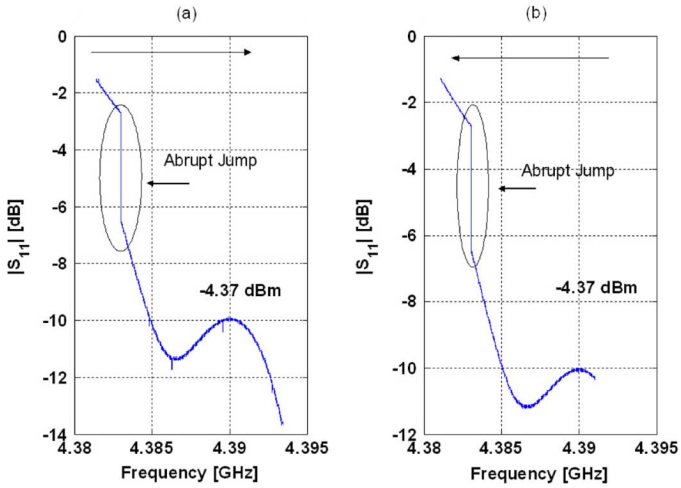

Fig. 8. (a) Forward continuous wave (CW) mode scan using NA, in a 12-MHz span around the left jump of the nonlinear resonance of B2. The scan includes 20 000 frequencies, which is equivalent to a frequency step of ~ 600 Hz between the data points. In spite of this small frequency step, the jump occurs between just two sequential frequencies. (b) A backward CW mode scan using NA, within a 10 MHz span around the left jump of the nonlinear resonance of B2. The scan includes 4000 frequencies, which is equivalent to a frequency step of ~ 2.5 kHz between the data points. Also for this case the jump occurs between just two sequential frequencies.

response generally lead to a hysteretic behavior at the vicinity of the bifurcations. In order to examine the resonance response dependence of these resonators on frequency, we have applied forward and backward frequency sweeps.

In Fig. 9, we show a representative frequency scan of B2 second mode, applied in both directions, featuring some interesting hysteretic behavior:

1) At low input powers -8.05 dBm and -8.04 dBm, the resonance is symmetrical and there is no hysteresis.

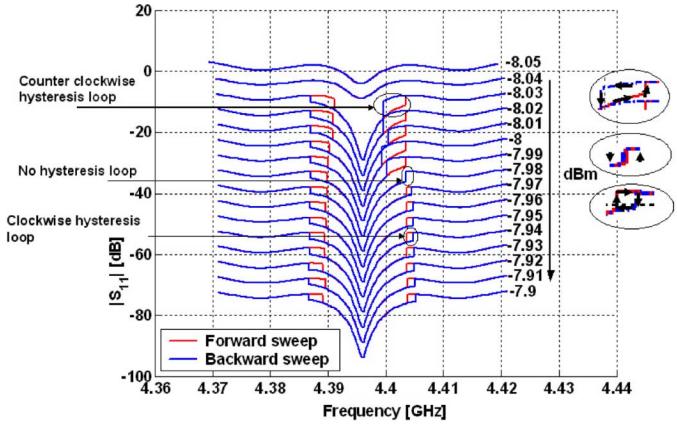

Fig. 9. Forward and backward scan measurement, performed using NA, measuring B2 second mode nonlinear resonance. Red line represents a forward scan whereas the blue line represents a backward scan. The graphs exhibit clear hysteresis loops forming at the vicinity of the jumps, and hysteresis loop changing direction as the input power is increased. Resonance curves corresponding to different input powers were shifted by a constant offset for clarity.

2) As the power is increased by 0.01 dBm to -8.03 dBm, two jumps occur at both sides of the resonance response and hysteresis loops form at the metastable regions.
3) As we continue to increase the input power gradually, the hysteresis loop associated with the right jump changes direction. At first it circulates counterclockwise between -8.03 dBm and -7.99 dBm, at -7.98 dBm the two opposed jumps at the right side meet and no hysteresis is detected. As we further increase the power, the right hysteresis loop appears again, circulating, this time, in the opposite direction, clockwise.

It is worth mentioning that the hysteresis loops changing direction are not unique to this resonator, or to the jump on the right side of the resonance. It appears also in the modes of B1, and it occurs at the left side jump of this resonance as well, though at different power level.

E. Multiple Jumps

Frequency sweep applied to B3 first resonance in both directions, exhibits yet another feature, in addition to the two jumps at the sides of the resonance curve, which we have seen earlier, there are another smaller jumps accompanied with hysteresis within the resonance lineshape, adding up to 3 jumps in each scan direction, and four hysteresis loops, as exhibited in Fig. 10.

F. Surface Impedance

Following surface impedance analysis carried in [2], [31], [34] which is generally used as an effective tool for investigating nonlinearity [10], [32], we try to quantify reactance and resistive changes, ΔX and ΔR, respectively, in the resonators, as a function of RF input power P_{RF}, using the following relations, $\Delta X(P_{\mathrm{RF}}) \propto 2\Delta f_0/f_0 = 2[f_0(P_{\min}) - f_0(P_{\mathrm{RF}})]/f_0(P_{\min})$ and $\Delta R(P_{\mathrm{RF}}) \propto \Delta(1/Q) = 1/Q(P_{\mathrm{RF}}) - 1/Q(P_{\min})$ [2], where f_0 is the resonance frequency determined from the minimum of the resonance curve, Q is the quality factor of the resonator, and $P_{\min}$ is the onset of nonlinearity input power. Whereas the first expression defines the relative frequency shift

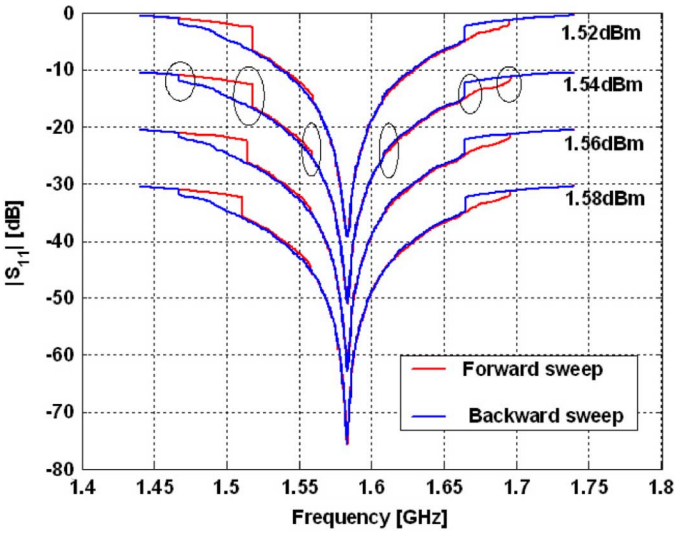

Fig. 10. S_{11} parameter measurement of the first resonance of B3 at input powers 1.52 dBm through 1.58 dBm in steps of 0.02 dBm using forward and backward CW mode scan of NA employing 2000 measurement points in each direction. Graph shows clearly three jumps within the band of the resonance in each direction. Resonance curves corresponding to different input powers were shifted by a constant offset for clarity.

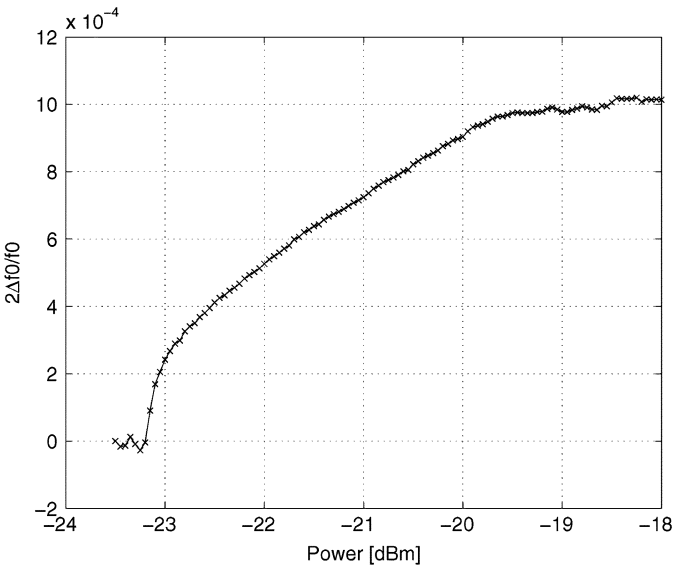

Fig. 11. Relative frequency shift $2\Delta f_0/f_0$ as a function of RF input power, corresponding to B1 third resonance frequency.

of the resonance, the second expression defines the difference in the microwave losses of the resonator. The quality factor Q of the resonators in the nonlinear regime was calculated using a Lorentzian fit applied to the $|S_{11}|^2$ data (the square amplitude of the reflection parameter) in the vicinity of the resonance [36]. Nevertheless, this approach does not enable us to calculate unambiguously the Q factor of the resonance curves which are extremely asymmetrical and do not resemble Lorentzians in the vicinity of the resonance [2], [28], such as those shown in Fig. 3. Therefore, the graph exhibiting $\Delta(1/Q)$ for B1 resonance is not plotted here. In Figs. 11 and 12(a), we show the

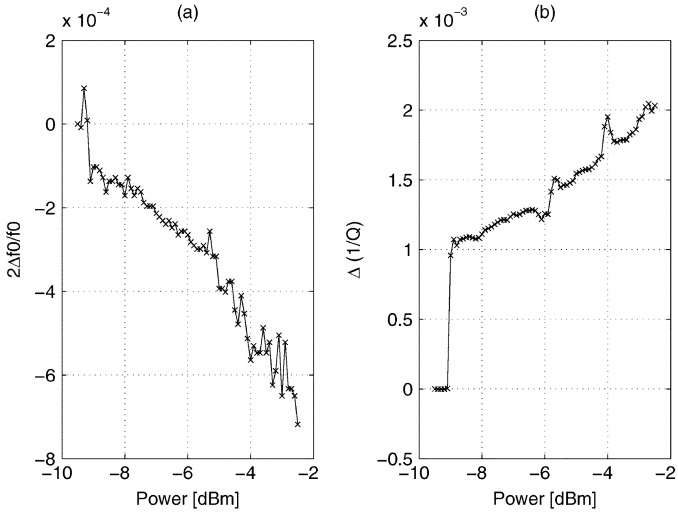

Fig. 12. (a) Relative frequency shift $2\Delta f_0/f_0$. (b) Relative microwave losses $\Delta(1/Q)$. Both graphs correspond to B2 second resonance frequency and are given as a function of RF input power.

$2\Delta f_0/f_0$ ratio calculated for B1 and B2 resonators respectively, whereas in Fig. 12(b), we show the difference ratio $\Delta(1/Q)$ for B2 resonator.

In Fig. 11, we observe a steep decrease in the resonance frequency at about -23 dBm, followed by a gradual shift of the resonance towards the lower frequencies up till -19.5 dBm, above which a plateau in the resonance frequency is observed. Whereas in Fig. 12(a) we measure a step in the resonance frequency at about -9 dBm, followed by a gradual increase untill -2 dBm. As to the relative losses $\Delta(1/Q)$, in Fig. 12(b), representing the second resonance of B2, the relative losses jumps at the onset of nonlinearity ~ -9 dBm and afterwords changes gradually as the input power increases.

Although Figs. 11 and 12 do not provide a clear coherent picture as to the physical origin of the observed nonlinearities, one can verify easily that these results differ from the resonance nonlinearities presented, for example, in [2], [10], [28], [31] exhibiting nonlinear effects which can be explained in terms of one dimensional Duffing oscillator equation [7], [37].

VI. Comparison with Duffing Oscillator Nonlinearity

In general hysteretic behavior in superconducting films is caused by one of the following physical nonlinear mechanisms: pair breaking, intrinsic nonlinearity [7], heating effects [13], vortex dynamics [34], and Josephson junctions [38]–[40]. *Oates et al.* in [37], showed that inductance change ΔL can lead to hysteretic behavior in the resonance response, whereas resistance change ΔR tends to suppress it (where ΔL and ΔR are given by the following relations $L = L_0 + \Delta L(I/I_c)^2, R = R_0 + \Delta R(I/I_c)^2$ [7], where I is the total current, $I_c$is the critical current, L_0, R_0 are the zero order inductance and resistance per unit length respectively). However, substituting L (inductance per unit length) and R (resistance per unit length) of the form $L = L_0 + \Delta L(I/I_c)^2, R = R_0 + \Delta R(I/I_c)^2$ into the transmission line equations given by $\partial I/\partial z = -C\partial V/\partial t, \partial V/\partial z =$

$-L\partial I/\partial t - RI$ [7], where V is the voltage along the transmission line and C is the capacitance per unit length, leads eventually to Duffing oscillator nonlinearity, which qualitatively differ from our results.

The main differences can be summarized as follows.

1) Whereas Duffing oscillator nonlinearity is gradual and builds up as the input power is increased, these presented effects are sudden and demonstrate high sensitivity to input power on the order of 0.01 dBm. (Figs. 3, 4, 9).
2) In Duffing oscillator nonlinearity, we observe (with Nb resonators) one jump and one or no hysteresis loop in the resonance lineshape, whereas in these resonators we observe two and sometimes more jumps and hysteresis loops. (Figs. 9 and 10).
3) In Duffing oscillator nonlinearity the hysteresis loop keeps its circulation direction, whereas in the presented results, the hysteresis loops may change direction. (Fig. 9).
4) These nonlinear effects may lead to critical coupling condition in some resonances. (Figs. 3 and 4).
5) Above some input power level the resonance becomes symmetrical again unlike Duffing oscillator nonlinearity. (Figs. 3 and 4).

VII. Nonlinear Mechanism Modeling

In attempt to account for some of the unusual nonlinear effects presented earlier, we consider herein a hypothesis according to which weak links (WL) forming at the boundaries of the granular NbN columnar structure [24]–[26] are the main source of the nonlinearities. WL, as it is well known, is a general term which represents a wide variety of "material defects," such as impurities, edge defects, built in Josephson junctions, insulating layers, grain boundaries, voids, and weak superconducting points [1]. Under certain conditions and circulating RF currents these WL can interrupt the shielding supercurrents and as a result affect the conductivity [41], the resonance mode and the losses inside the resonator. Thus, in this section we will consider a simple model where local heating mechanism acts on WL in the NbN films and switch them between normal and superconducting states [42]. This switching hypothesis is partly supported by Fig. 13, where the same experimental data of Fig. 9, have been redrawn while canceling the vertical offset between the different resonance curves. The resulting plot in Fig. 13, exhibits clearly abrupt transitions between two resonance curves.

For the purpose of modeling, consider a resonator driven by a weakly coupled feedline carrying an incident coherent tone $b^{\rm in}e^{-i\omega_p t}$, where $b^{\rm in}$ is a constant complex amplitude and ω_p is the drive angular frequency. The mode amplitude inside the resonator A can be written as $A = Be^{-i\omega_p t}$, where $B(t)$ is a complex amplitude, which is assumed to vary slowly on the time scale of $1/\omega_p$. In this approximation and while disregarding noise, the equation of motion of B reads [36]

$$\frac{dB}{dt} = [i(\omega_p - \omega_0) - \gamma]\, B - i\sqrt{2\gamma_1 1} b^{\rm in} \tag{2}$$

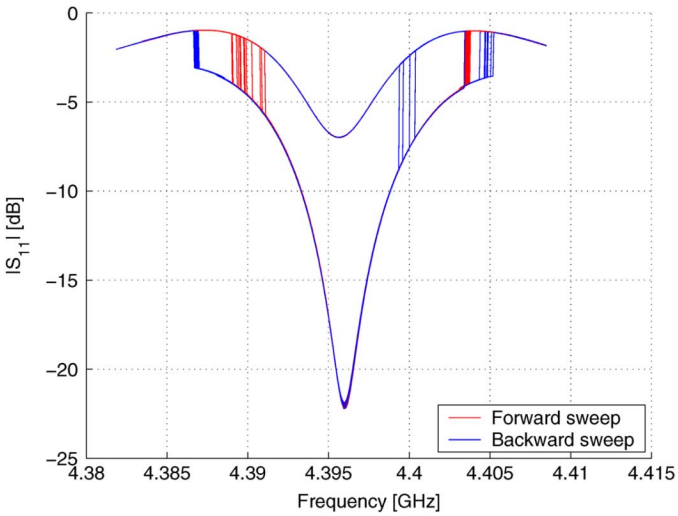

Fig. 13. Redrawing the experimental data of Fig. 9, while canceling the vertical offset between the graphs. The plot shows clear transitions between two resonance curves.

where ω_0 is the angular resonance frequency, $\gamma = \gamma_1 + \gamma_2$, where γ_1 is the coupling constant between the resonator and the feedline, and γ_2 is the damping rate of the mode.

In terms of the dimensionless time $\tau = \omega_0 t$, (2) reads

$$\frac{dB}{d\tau} = \frac{i(\omega_p - \omega_0) - \gamma}{\omega_0}(B - B_\infty) \tag{3}$$

where

$$B_\infty = \frac{i\sqrt{2\gamma_1} b^{\rm in}}{i(\omega_p - \omega_0) - \gamma}. \tag{4}$$

The output signal $a^{\rm out}$ reflected off the resonator can be written as $a^{\rm out} = b^{\rm out}e^{-i\omega_p t}$. The input–output relation relating the output signal to the input signal is given by [43]

$$\frac{b^{\rm out}}{\sqrt{\omega_0}} = \frac{b^{\rm in}}{\sqrt{\omega_0}} - i\sqrt{\frac{2\gamma_1}{\omega_0}} B. \tag{5}$$

Whereas the total power dissipated in the resonator Q_t can be expressed as [36]

$$Q_t = h\omega_0 2\gamma_2 E \tag{6}$$

where $E = |B|^2$.

Furthermore, consider the case where the nonlinearity is originated by a local hot spot in the stripline resonator. If the hot spot is assumed to be sufficiently small, its temperature T can be considered homogeneous. The temperature of other parts of the resonator is assumed be equal to that of the coolant T_0. The power Q heating up the hot spot is given by $Q = \alpha Q_t$ where $0 \leqslant \alpha \leqslant 1$.

The heat balance equation reads

$$C\frac{dT}{dt} = Q - W \tag{7}$$

where C is the thermal heat capacity, $W = H(T - T_0)$ is the power of heat transfer to the coolant, and H is the heat transfer coefficient. Defining the dimensionless temperature

$$\Theta = \frac{T - T_0}{T_c - T_0} \tag{8}$$

where T_c is the critical temperature, one has

$$\frac{d\Theta}{d\tau} = -g(\Theta - \Theta_\infty) \tag{9}$$

where

$$\Theta_\infty = \frac{2\alpha\gamma_2\rho E}{\omega_0 g} \tag{10}$$

$$\rho = h\omega_0 C(T_c - T_0) \tag{11}$$

$$g = \frac{H}{C\omega_0}. \tag{12}$$

The resonance frequency ω_0, the damping rates γ_1, γ_2, and α are assumed to have a step function dependence on the temperature

$$\omega_0 = \begin{cases} \omega_{0s}, & \Theta < 1 \\ \omega_{0n}, & \Theta > 1 \end{cases} \tag{13}$$

$$\gamma_1 = \begin{cases} \gamma_{1s}, & \Theta < 1 \\ \gamma_{1n}, & \Theta > 1 \end{cases} \tag{14}$$

$$\gamma_2 = \begin{cases} \gamma_{2s}, & \Theta < 1 \\ \gamma_{2n}, & \Theta > 1 \end{cases} \tag{15}$$

$$\alpha = \begin{cases} \alpha_s, & \Theta < 1 \\ \alpha_n, & \Theta > 1. \end{cases} \tag{16}$$

.

While disregarding noise, the coupled (3) and (9) may have, in general, up to two different steady state solutions. A superconducting steady state of the WL exists when $\Theta_\infty < 1$, or alternatively when $E < E_s$, where $E_s = gC(T_c - T_0)/2\alpha_s\gamma_{2s}h$. Similarly, a normal steady state of the WL exists when $\Theta_\infty < 1$, or alternatively when $E > E_n$, where $E_n = gC(T_c - T_0)/2\alpha_n\gamma_{2n}h$.

Moreover, the reflection coefficient S_{11} of the resonant in steady state is given by [36]

$$S_{11}(\omega) = \frac{b^{\text{out}}}{b^{\text{in}}} = \frac{\gamma_2 - \gamma_1 - i(\omega_p - \omega_0)}{\gamma_2 + \gamma_1 - i(\omega_p - \omega_0)}. \tag{17}$$

Thus, WL switching between the superconducting and the normal states cause simultaneous switching of $\omega_0, \gamma_1, \gamma_2, \alpha$ parameters which in turn change the resonance lineshape abruptly and result in hysteretic behavior in the bistable region.

In general, the heat capacity C can be expressed as $C = C_v t A_{\text{eff}}$, where C_v is the specific heat of NbN ($2.7\cdot10^{-3}$ J cm^{-3} K^{-1} [44]), t is the thickness of the film, and A_{eff} is the effective area of the hot spot. By further assuming that the generated heat is cooled mainly down the substrate rather than along the film [45], [46], the heat transfer coefficient H reads $H = \sigma A_{\text{eff}}$, where α is the thermal surface conductance between the superconducting film and the substrate. To obtain an estimate for A_{eff}, we evaluate the total dissipated power Q_t in the resonator [given by (6)] at the WL superconducting state threshold E_s : $Q_t = gC(T_c - T_0)\omega_0/\alpha_s$. Using (12) and $H = \sigma A_{\text{eff}}$ relation yield

$$A_{\text{eff}} \simeq \frac{Q_t}{\sigma(T_c - T_0)} \tag{18}$$

where α_s is assumed to be of order unity. To evaluate A_{eff} for the second mode of B2 at the onset power of nonlinearity $P_W \sim 1.6\cdot10^{-4}$ W (corresponding to ~ -8.03 dBm of Fig. 9), we relate Q_t to P_W at the jump frequency, using $Q_t = (1-r_v^2)P_W \simeq 8\cdot10^{-5}$ W. Substituting Q_t and the following resonator parameters: $T_c = 6.8$ K, $T_0 = 4.2$ K, $\sigma = 2$ W cm^{-2} K^{-1} at 4.2 K [46], [47], in (18) yield $A_{\text{eff}} \simeq 1.5\cdot 10^{-5}$ cm^2. Substituting this result in C and H expressions gives $C \simeq 1.2\cdot 10^{-12}$ J/K, $H \simeq 3\cdot10^{-5}$ W/K. Whereas direct substitution in (11) and (12) yield the dimensionless parameters $\rho \simeq 9\cdot10^{-13}, g \simeq 9\cdot10^{-4}$ respectively.

Next, we numerically simulate the unusual hysteretic behavior of B2 second mode ($\omega_{0n} = 2\cdot\pi\cdot 4.395$ GHz) shown in Fig. 9 using this model and the parameters derived above. In Fig. 14, we show one of the simulation results corresponding

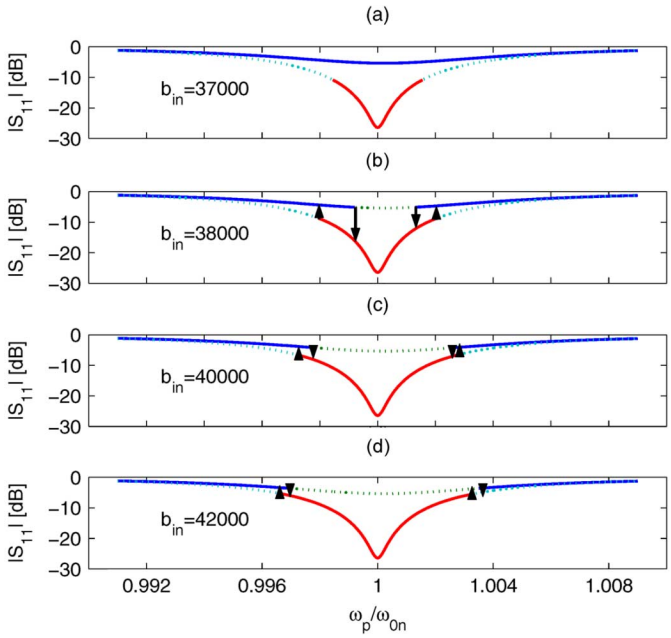

Fig. 14. Simulated resonance response. Plots (a)–(d) correspond to an increasing drive amplitude b^{in}. Solid lines represent valid steady state solutions whereas the dotted lines represent invalid solutions. Red/cyan lines represent the normal WL solutions, whereas the blue/green lines represent the superconducting WL solutions. Black arrows show the direction of the hysteresis loops in the different cases. Parameters that were used in the simulation are: $\omega_{0s}/\omega_{0n} = 1.00023, \gamma_{1n}/\omega_{0n} = 2.5\cdot10^{-3}, \gamma_{1s}/\omega_{0n} = 1.5\cdot10^{-3}, \gamma_{2n}/\omega_{0n} = 2.75\cdot10^{-3}, \gamma_{2s}/\omega_{0n} = 5\cdot10^{-3}, \alpha_n = 0.8, \alpha_s = 1, g = 9\cdot10^{-4}, \rho = 9\cdot10^{-13}$.

to increasing values of b^{in}, the drive amplitude. The simulation parameters used are listed in the figure caption. The blue solid line represents the valid superconducting WL steady state solution ($E < E_s$), while the green dotted line represents the invalid steady state solution ($E > E_s$). Similar lines are plotted for the normal WL steady state solution. The red solid line represents the valid solution ($E > E_n$), while the cyan dotted line represents the invalid one ($E < E_n$). For the simulation parameters chosen in plot (a), the superconducting WL steady state solution is valid at all frequencies (the blue line) and thus the system follows this resonance lineshape as the frequency is scanned back and forth. In plot (b) corresponding to a higher amplitude drive, the superconducting WL steady state solution is not valid at all frequencies, thus as the superconducting WL solution becomes invalid under forward frequency sweep, the system jumps to the valid normal WL steady state solution as indicated by the downward arrow at the left side of the resonance. As we continue to sweep the frequency forward, another jump occurs at the right side of the resonance back to the blue solid line (indicated by the upward arrow) as the normal WL steady state solution becomes invalid. Sweeping the frequency in the backward direction exhibits hysteresis in the response lineshape, since the opposed jumps differ, as can be clearly seen in plot (b). As we increase the amplitude drive b^{in} further [see plot (c)], we successfully obtain a case where the two opposed jumps at the right side of the resonance are in close proximity of each other. Whereas in plot (d) corresponding to a higher amplitude drive one gets a frequency region (see the right side of the resonance) where no steady state solution is valid. This result may potentially explain the third enlarged hysteresis loop which appears in Fig. 9, where the two opposed jumps occur earlier in each frequency sweep direction. That is if one assumes the existence of additional two valid solutions within the "invalid region" which the system jumps to, and which coincide with the existing valid solutions outside this region. Such additional solutions can possibly originate from another WL becoming active at these higher amplitude drives. Moreover the assumption of different WL becoming active may be needed also to account for the multiple jumps feature presented in Figs. 5 and 10.

VIII. Conclusion

In the course of this experimental work, we have fabricated several stripline NbN resonators dc-magnetron sputtered on sapphire substrates at room temperature implementing different geometries. The resonators have exhibited similar and unusual nonlinear effects in their resonance response curves. The onset of the nonlinear effects in these NbN resonators varied between the different resonators, but usually occurred at relatively low microwave powers, typically 2–3 orders of magnitude lower than Nb for example. Among the nonlinear effects observed: abrupt and multiple jumps in the resonance curve, power dependent resonance frequency shift, hysteresis loops in the vicinity of the jumps, hysteresis loops changing direction, and critical coupling phenomenon. Weak links forming in the NbN films are hypothesized as the source of the nonlinearities. Further study of these effects under other modes of operation and measurement conditions would be carried in the future, in order to substantiate our understanding of these extraordinary effects.

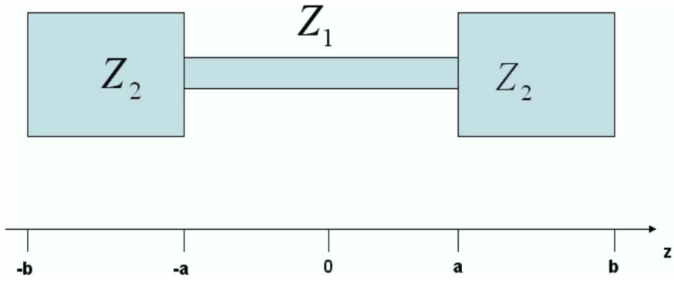

Fig. 15. Geometry model.

Appendix I
Resonance Frequency Calculation of B1, B2, B3 Resonators

The calculation process of the resonance frequencies of B1 and B2 makes use of opposite traveling voltage-current waves method [48], [49]. For this purpose, we model B1 and B2 resonators as a straight transmission line extending in the z-direction with two characteristic impedance regions Z_1 and Z_2 as shown in Fig. 15.

The equivalent voltage along the resonator transmission line would be given, in general, by a standing waves expression in the form

$$V(z) = \begin{cases} A_+ \cos\beta(z-a) + B_+ \sin\beta(z-a) & z\epsilon(a,b) \\ A\cos\beta z + B\sin\beta z & z\epsilon(-a,a) \\ A_- \cos\beta(z+a) + B_- \sin\beta(z+a) & z\epsilon(-b,-a) \end{cases} \tag{19}$$

where β ($= 2\pi f\sqrt{\varepsilon_r}/c$) is the propagation constant along the transmission line, and A_+, B_+, A, B, A_-, B_- are constants that can be determined using boundary conditions. However due to the symmetry of the problem $z \longleftrightarrow -z$, we expect the solutions to have defined parity, where $V(z) = V(-z)$ for symmetric solution and $V(z) = -V(-z)$ for antisymmetric solution. Thus by taking advantage of this property and demanding that $V(z)$ be continuous at $z = a$ and $z = -a$, one gets:

$$V_{\text{sym}}(z) = \begin{cases} \cos\beta a\cos\beta(z-a) & \\ +B_s\sin\beta(z-a), & z\epsilon(a,b) \\ \cos\beta z, & z\epsilon(-a,a) \\ \cos\beta a\cos\beta(z+a) & \\ -B_s\sin\beta(z+a), & z\epsilon(-b,-a) \end{cases}$$

$$V_{\text{anti}}(z) = \begin{cases} \sin\beta a\cos\beta(z-a) & \\ +B_a\sin\beta(z-a), & z\epsilon(a,b) \\ \sin\beta z, & z\epsilon(-a,a) \\ -\sin\beta a\cos\beta(z+a) & \\ +B_a\sin\beta(z+a), & z\epsilon(-b,-a) \end{cases}$$

where $V_{\text{sym}}(z)$ stands for the symmetric solution whereas $V_{\text{anti}}(z)$ for the antisymmetric solution. To calculate the value

of the new constants B_s, B_a, we require that the equivalent current $I(z)$ along the transmission line, which is given by $I(z) = (i/\beta Z_i)dV/dz$ where Z_i is the characteristic impedance of the line (in the $i = 1, 2$ region), be continuous at $z = a$ and $z = -a$. Following this requirement one gets $B_s = -\eta \sin(\beta a)$ and $B_a = \eta \cos(\beta a)$, where $\eta = Z_2/Z_1$.

A. B1 Resonator

Since the resonator ends are shorted we demand $V(b) = V(-b)$.

The symmetric case:

In this case, we either have maximum or minimum at $V(b)$ thus we get $I(b) = 0$, yielding the following condition on the resonance frequencies

$$\cos(\beta a)\sin(\beta(b-a)) + \eta \sin(\beta a)\cos(\beta(b-a)) = 0 \quad (20)$$

The antisymmetric case:

From the antisymmetric $V(-b) = -V(-b)$ and the continuity $V(b) = V(-b)$ conditions, we get $V(b) = V(-b) = 0$, which yields

$$\sin(\beta a)\cos(\beta(b-a)) + \eta \cos(\beta a)\sin(\beta(b-a)) = 0 \quad (21)$$

Substituting the following numerical values $\eta = Z_2/Z_1 = 0.5, l_1 = a = 13$ mm, $l_2 = b - a = 6.5$ mm into the above resonance frequency conditions and solving for frequencies below 10 GHz, yield the following solutions (2.5035 GHz, 5.697 GHz, 8.1647 GHz) for the symmetric case, and (2.9804 GHz, 5.1786 GHz, 8.1647 GHz) for the antisymmetric case, with doubly degenerate mode at 8.1647 GHz. By comparing these calculated resonances to the directly measured resonances of B1 resonator, obtained using a broadband S_{11} measurement (2.5812 GHz, 5.6304 GHz, 8.4188 GHz), we find that the excited resonances correspond to the symmetrical case only. The antisymmetric modes do not get excited because they have a voltage node at the feedline position.

B. B2 Resonator

Since the resonator ends are open-circuited, we demand $I(b) = I(-b) = 0$.

The symmetric case:

We require that the current associated with the symmetric voltage, vanishes:

$$\cos(\beta a)\sin[\beta(b-a)] + \eta \sin(\beta a)\cos[\beta(b-a)] = 0 \quad (22)$$

The antisymmetric case:

We require that the current associated with the antisymmetric voltage, vanishes:

$$-\sin(\beta a)\sin(\beta(b-a)) + \eta \cos(\beta a)\cos\beta(b-a) = 0 \quad (23)$$

Substituting the following numerical values $\eta = Z_2/Z_1 = 49.9/10.4 = 4.79, l_1 = a = 11.97$ mm, $l_2 = b - a = 6.43$ mm into the above resonance frequency conditions and solving for frequencies below 10 GHz, yield the following solutions (2.6486 GHz, 6.0288 GHz, 8.5588 GHz) for the symmetric case, and (1.1763 GHz, 4.3698 GHz, 7.4597 GHz, 9.7778 GHz for the antisymmetric case. By comparing these calculated resonances to the directly measured resonances of B2 resonator, obtained using a broadband S_{11} measurement (2.5152 GHz, 4.425 GHz, 6.3806 GHz, 8.176 GHz), we find a good agreement between the two results. The missing resonances do not get excited apparently because of the coupling location of the feedline relative to the resonator.

C. B3 Resonator

B3 resonator, in contrast, showed some larger discrepancy between the measured value for the first mode $\sim$1.6 GHz (seen in Fig. 5) and the theoretical value $f_1 = 2.4462$ GHz calculated according to the approximated equation:

$$f_n = \frac{nc}{2l\sqrt{\varepsilon_r}} \quad (24)$$

where n is the mode number, c is the light velocity, l is the open-circuited line length ($\simeq$20 mm), and ε_r is the relative dielectric coefficient of the sapphire ($\simeq$9.4).

ACKNOWLEDGMENT

E. Buks would like to thank M. L. Roukes for supporting the early stage of this research and for many helpful conversations and invaluable suggestions. Very helpful conversations with G. Eisenstein, O. Gottlieb, G. Koren, E. Polturak, and B. Yurke are also gratefully acknowledged.

REFERENCES

[1] J. Halbritter, "RF residual losses,surface impedance and granularity in superconducting cuprates," *J. Appl. Phys.*, vol. 68, p. 6315, Dec. 1990.

[2] M. A. Golosovsky, H. J. Snortland, and M. R. Beasley, "Nonlinear microwave properties of superconducting Nb microstrip resonators," *Phys. Rev. B.*, vol. 51, p. 6462, Mar. 1995.

[3] S. K. Yip and J. A. Sauls, "Nonlinear Meissner effect in CuO Superconductors," *Phys. Rev. Lett.*, vol. 69, p. 2264, Oct. 1992.

[4] J. Wosik, L.-M. Xie, J. Mazierska, and R. Grabovickic, "Influence of columnar defects on surface resistance of YBaCuO superconducting thin films; nonlinear effects," *Appl. Phys. Lett.*, vol. 75, p. 1781, Sept. 1999.

[5] D. E. Oates, M. A. Hein, P. J. Hirst, R. G. Humphreys, G. Koren, and E. Polturak, "Nonlinear microwave surface impedance of YBCO films: Latest results and present understanding," *Physica C*, vol. 372, pp. 462–468, 2002.

[6] S. M. Anlage, W. Hu, C. P. Vlahacos, D. Steinhauer, B. J. Feenstra, S. K. Dutta, A. Thanawalla, and F. C. Wellstood, "Microwave nonlinearities in high-T_c superconductors: The truth is out there," *J. Supercond.*, vol. 12, p. 353, 1999.

[7] T. Dahm and D. J. Scalapino, "Theory of intermodulation in a superconducting microstrip resonator," *J. Appl. Phys.*, vol. 81, p. 2002, Feb. 1997.

[8] D. E. Oates, S.-H. Park, M. A. Hein, P. J. Hirst, and R. G. Humphreys, "Intermodulation distortion and third-harmonic generation in YBCO films of varying oxygen content," *IEEE Trans. Appl. Supercond.*, vol. 13, no. 2, pp. 311–314, Jun. 2003.

[9] T. Dahm and D. J. Scalapino, "Analysis and Optimization of intermodulation in high T_c superconducting microwave filter design," *IEEE Trans. Appl. Supercond.*, vol. 8, no. 4, pp. 149–157, Dec. 1998.

[10] C. C. Chen, D. E. Oates, G. Dresselhaus, and M. S. Dresselhaus, "Nonlinear electrodynamics of superconducting NbN and Nb thin films at microwave frequencies," *Phys. Rev. B.*, vol. 45, p. 4788, Mar. 1992.

[11] J. Wosik, L.-M. Xie, J. H. Miller, Jr., S. A. Long, and K. Nesteruk, "Thermally-induced nonlinearities in the surface impedance of superconducting YBCO thin films," *IEEE Trans. Appl. Supercond.*, vol. 7, no. 2, pp. 1470–1473, Jun. 1997.

[12] B. A. Willemsen, J. S. Derov, J. H. Silva, and S. Sridhar, "Nonlinear response of suspended high temperature superconducting thin film microwave resonators," *IEEE Trans. Appl. Supercond.*, vol. 5, no. 2, pp. 1753–1755, Jun. 1995.

[13] L. F. Cohen, A. L. Cowie, A. Purnell, N. A. Lindop, S. Thiess, and J. C. Gallop, "Thermally induced nonlinear behavior of HTS films at high microwave power," *Supercond. Sci. Technol.*, vol. 15, p. 559, 2002.

[14] A. M. Portis, H. Chaloupka, M. Jeck, and A. Pischke, "Power-induced switching of an HTS microstrip patch antenna," *Superconduct. Sci. Technol.*, vol. 4, no. 9, p. 436, Sep. 1991.

[15] S. J. Hedges, M. J. Adams, and B. F. Nicholson, "Power dependent effects observed for a superconducting stripline resonator," *Elect. Lett.*, vol. 26, no. 14, Jul. 1990.

[16] J. Wosik, L.-M. Xie, R. Grabovickic, T. Hogan, and S. A. Long, "Microwave power handling capability of HTS superconducting thin films: Weak links and thermal effects induced limitation," *IEEE Trans Appl. Supercond.*, vol. 9, no. 2, pp. 2456–2459, Jun. 1999.

[17] Z. Wang, A. Kawakami, Y. Uzawa, and B. Komiyama, "Superconducting properties and crystal structures of single-crystal niobium nitride thin films deposited at ambient substrate temperature," *J. Appl. Phys.*, vol. 79, p. 7837, Feb. 1996.

[18] D. D. Bacon, A. T. English, S. Nakahara, F. G. Peters, H. Schreiber, W. R. Sinclair, and R. B. van Dover, "Properties of NbN thin films deposited on ambient temperature substrates," *J. Appl. Phys.*, vol. 54, p. 6509, Jul. 1983.

[19] S. Thakoor, J. L. Lamb, A. P. Thakoor, and S. K. Khanna, "High T_c superconducting NbN films deposited at room temperature," *J. Appl. Phys.*, vol. 58, p. 4643, Dec. 1985.

[20] P. Yagoubov, G. Gol'tsman, B. Voronov, L. Seidman, V. Siomash, S. Cherednichenko, and E. Gershenzon, "The bandwidth of HEB mixers employing ultrathin NbN films on sapphire substrate," in *7th Int. Symp. Space Terahertz Technol.*, Mar. 1996, p. 290.

[21] A. C. Anderson, D. J. Lichtenwalner, and W. T. Brogan, "Process control for the low temperature deposition of niobium-nitride thin films," *IEEE Trans. Mag.*, vol. 25, no. 2, pp. 2084–2088, Mar. 1989.

[22] Y. Pellan, G. Dousselin, J. Pinel, and Y. U. Sohn, "Temperature and magnetic field dependence of NbN film resistivity: 3D weak localization effects," *J. Low Temp. Phys.*, vol. 78, p. 60, Jun. 1990.

[23] H. C. Jones, "Some properties of granular thin films of high-field superconductors," *Appl. Phys. Lett.*, vol. 27, p. 471, Oct. 1975.

[24] Y. M. Shy, L. E. Toth, and R. Somasundaram, "Superconducting properties, electrical resistivities, and structure of NbN thin films," *J. Appl. Phys.*, vol. 44, p. 5539, Dec. 1973.

[25] H. L. Hoetal, R. T. Kampwirth, K. E. Gray, D. W. Capone II, L. S. Chumbley, and M. MeshII, "Electron microscopy study of sputtered NbN films," *Ultramicroscopy*, vol. 22, p. 297, Apr. 1987.

[26] S. Isagawa, "RF superconducting properties of reactively sputtered NbN," *J. Appl. Phys.*, vol. 52, p. 921, Oct. 1980.

[27] D. E. Oates, A. C. Anderson, and P. M. Mankiewich, "Measurement of the surface resistance of $YBa_2Cu_3O_{7-x}$ thin films using stripline resonators," *J. Supercond.*, vol. 3, p. 251, 1990.

[28] D. E. Oates, A. C. Anderson, D. M. Sheen, and S. M. Ali, "Stripline resonator measurements of Z_s versus H_{RF} in $YBa_2Cu_3O_{7-x}$ thin films," *IEEE Trans. Microw. Theory Tech.*, vol. 39, no. 2, pp. 1522–1529, Sep. 1991.

[29] E. H. Rhoderick and E. M. Wilson, "Current distribution in thin superconducting films," *Nature*, vol. 194, p. 1167, Jun. 1962.

[30] R. Hu, G. L. Kerber, J. Luine, E. Ladizinsky, and J. Bulman, "Sputter deposition conditions and penetration depth in NbN thin films," *IEEE Trans. Appl. Supercond.*, vol. 13, no. 2, pp. 3288–3291, Jun. 2003.

[31] A. Andreone, A. Cassinese, A. Di Chiara, M. Lavarone, F. Palomba, A. Ruosi, and R. Vaglio, "Nonlinear microwave properties of Nb_3Sn sputtered superconducting films," *J. Appl. Phys.*, vol. 82, p. 1736, Aug. 1997.

[32] P. P. Nguyen, D. E. Oates, G. Dresselhaus, and M. S. Dresselhaus, "Nonlinear surface impedance for $YBa_2Cu_3O_{7-x}$ thin films: Measurements and a coupled-grain model," *Phys. Rev. B*, vol. 48, p. 6400, Sep. 1993.

[33] P. P. Nguyen, D. E. Oates, G. Dresselhaus, M. S. Dresselhaus, and A. C. Anderson, "Microwave hysteretic losses in $YBa_2Cu_3O_{7-x}$ and NbN thin films," *Phys. Rev. B*, vol. 51, p. 6686, Mar. 1995.

[34] H. Xin, D. E. Oates, G. Dresselhaus, and M. S. Dresselhaus, "Microwave-frequency vortex dynamics in YBCO grain boundaries," *J. Supercond.*, vol. 14, p. 637, Oct. 2001.

[35] D. E. Oates, H. Xin, G. Dresselhaus, and M. S. Dresselhaus, "Intermodulation distortion and Josephson vortices in YBCO bicrystal grain boundaries," *IEEE Trans. Appl. Supercond.*, vol. 11, no. 1, pp. 2804–2807, Mar. 2001.

[36] B. Yurke and E. Buks, "Performance of capacity-parametric amplifiers, employing Kerr nonlinearities in the presence of two-photon loss," *J. Lightw. Technol.*, vol. 24, no. 12, Dec. 2006, to be published.

[37] J. H. Oates, R. T. Shin, D. E. Oates, M. J. Tsuk, and P. P. Nguyen, "A nonlinear transmission line model for superconducting stripline resonators," *IEEE Trans. Appl. Superconduct.*, vol. 3, no. 1, pp. 17–22, Mar. 1993.

[38] H. Prance, T. D. Clark, R. Whiteman, R. J. Prance, M. Everitt, P. Stiffel, and J. F. Ralph, "Pinch resonances in a radio-frequency-driven superconducting-quantum-interference-device ring-resonator system," *Phys. Rev. E*, vol. 64, p. 016208, Jun. 2001.

[39] R. Whiteman, J. Diggins, V. Schollmann, T. D. Clark, R. J. Prance, H. Prance, and J. F. Ralph, "Opposed (hammerhead) bifurcations in the resonant lineshape of a strongly driven SQUID ring-tank circuit system," *Phys. Lett. A*, vol. 234, p. 205, Sept. 1997.

[40] R. J. Prance, R. Whiteman, T. D. Clark, H. Prance, V. Schollmann, J. F. Ralph, S. Al-Khawaja, and M. Everitt, "Nonlinear multilevel dynamics of a coupled SQUID ring-resonator system in the hysteretic regime," *Phys. Rev. Lett.*, vol. 82, p. 5401, Jun. 1999.

[41] J. Halbritter, "Granular superconductors and their intrinsic and extrinsic surface impedance," *J. Supercond.*, vol. 8, p. 691, 1995.

[42] A. VI. Gurevich and R. G. Mints, "Self-heating in normal metals and superconductors," *Rev. Mod. Phys.*, vol. 59, p. 941, Oct. 1987.

[43] C. W. Gardinar and M. J. Collett, "Input and output in damped quantum systems: Quantum stochastic differential equations and the master equation," *Phys. Rev. A*, vol. 31, p. 3761, June 1985.

[44] K. Weiser, U. Strom, S. A. Wolf, and D. U. Gubserm, "Use of granular NbN as a superconducting bolometer," *J. Appl. Phys.*, vol. 52, p. 4888, Jul. 1981.

[45] A. M. Kadin and M. W. Johnson, "Nonequilibrium photon-induced hotspot: A new mechanism for photodetection in ultrathin metalic films," *Appl. Phys. Lett.*, vol. 69, p. 3938, Dec. 1996.

[46] W. J. Skocpol, M. R. Beasley, and M. Tinkham, "Self-heating hotspots in superconducting thin-film microbridges," *J. Appl. Phys.*, vol. 45, p. 4054, Sep. 1974.

[47] M. W. Johnson, A. M. Herr, and A. M. Kadin, "Bolometric and nonbolometric infrared photoresponses in ultrathin superconducting NbN films," *J. Appl. Phys.*, vol. 79, p. 7069, May 1996.

[48] P. Gardner, D. K. Paul, and K. P. Tan, "Planar microstrip ring resonator filters," in *Colloquium on Microwave Filters and Antennas for Personal Communication Systems Digest*, Feb. 1994, vol. 6, pp. 1–6.

[49] K. Chang, S. Martin, F. Wang, and J. L. Klein, "On the study of microstrip ring and varactor-tuned ring circuits," *IEEE Trans. Microw. Tech.*, vol. 35, no. 12, pp. 1288–1295, Dec. 1987.

Baleegh Abdo (S'02) was born in Haifa, Israel, in 1979. He received the B.Sc. degree in computer engineering and the M.Sc. degree in electrical engineering, in 2002 and 2004, respectively, from the Technion-Israel Institute of Technology, Haifa, Israel, where he is currently he is working toward the Ph.D. degree in electrical engineering. His graduate research interests are nonlinear effects in superconducting resonators in the microwave regime, resonator coupling, and quantum qubits.

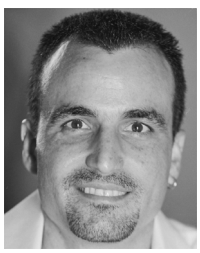

Eran Arbel-Segev was born in Haifa, Israel, in 1975. He received the B.Sc. degree in computer engineering and the M.Sc. degree in electrical engineering, in 2003 and 2006, respectively, from the Technion-Israel Institute of Technology, Haifa, Israel, where he is currently working toward the Ph.D. degree in electrical engineering. His research is focused on parametric gain in superconducting microwave resonators.

Oleg Shtempluck was born in Moldova, in 1949. He received the M.Sc. degree in electronic engineering from the Physical Department, Chernovtsy State University, Ukraine (former Soviet Union), in 1978. His research concerned semiconductors and dielectrics.

From 1983 to 1992, he was a team leader in the division of design engineering in Electronmash and from 1992 to 1999, he worked as stamp and mould design engineer at Ikar Company, both in Ukraine. Currently, he is working as a laboratory engineer in Microelectronics Research Center, Technion—Israel Institute of Technology, Haifa, Israel.

Eyal Buks received the B.Sc. degree in mathematics and physics from the Tel-Aviv University, Tel-Aviv, Israel, in 1991 and the M.Sc. and Ph.D. degrees in physics from the Weizmann Institute of Science, Israel, in 1994 and 1998, respectively. His graduate work concentrated on interference and dephasing in mesoscopic systems.

From 1998 to 2002, he worked at the California Institute of Technology (Caltech), Pasadena, as a Postdoctoral Scholar studying experimentally nanomachining devices. He is currently a Senior Lecturer at the Technion-Israel Institute of Technology, Haifa. His current research is focused on nanomachining and mesoscopic physics.